2D hole gas mobility at diamond/insulator interface

G. Daligou, J. Pernot

Applied Physics Letters ARTICLE scitation.org/journal/apl

2D hole gas mobility at diamond/insulator interface

Cite as: Appl. Phys. Lett. **116**, 162105 (2020); doi: 10.1063/5.0002768
Submitted: 27 January 2020 · Accepted: 27 March 2020 ·
Published Online: 22 April 2020

G. Daligou and J. Pernot[a)]

AFFILIATIONS

Univ. Grenoble Alpes, CNRS, Institut Néel, 38000 Grenoble, France

[a)]Author to whom correspondence should be addressed: julien.pernot@neel.cnrs.fr

ABSTRACT

The hole mobility of two-dimensional (2D) gas at (001) and (111) diamond/insulator interfaces is investigated theoretically and compared with experimental data from the literature. It is shown that the surface impurity scattering is the limiting mechanism at room temperature in most of the H-terminated diamond field effect transistors, where the negative charges created by transfer doping are in the vicinity of the 2D gas. By repelling the negative charges at the metal/insulator interface, as recently reported for the (111) h-BN/diamond interface, we demonstrate that it is possible to achieve high mobility values of the order of 3000 $cm^2/V\,s$ when a pure phonon scattering occurs. This work confirms the potential of two-dimensional hole gas diamond field effect transistors for high power and high frequency applications.

Diamond is a fascinating semiconductor with exceptional physical properties such as a wide bandgap, a high breakdown electric field (up to 20 MV/cm),[1] an outstanding thermal conductivity (20 W/cm/K),[2] and high carrier mobilities (hole: 2000 $cm^2/V\,s$[3] and electron: 1000 $cm^2/V\,s$[4]). These exceptional properties or, more precisely, the combination of some of these properties make diamond an ideal semiconductor for high power and/or high frequency electronics, which should surpass other materials like silicon, silicon carbide, or gallium nitride.[5] Numerous diamond field effect transistors (FETs) are under investigation: H-terminated accumulation FETs,[6] O-terminated inversion channel FETs,[7] metal-semiconductor FETs,[8] deep depletion FETs,[9] and junction FETs.[10]

For some of them, the conducting channel of the ON-state is composed of a two-dimensional (2D) carrier gas at the diamond/insulator interface, i.e., accumulation and inversion channel FETs. However, the 2D hole channel mobility values reported in the literature range between 3 and 300 $cm^2/V\,s$[11] and are systematically lower than the maximum hole mobility value reported in bulk material (2000 $cm^2/V\,s$).[3] This discrepancy is still not understood, and so the potential of 2D hole gas diamond FETs is still doubtful. Recently, Sasama *et al.*[12] reported a higher mobility value around 500 $cm^2/V\,s$ for (111) diamond FETs with a monocrystalline h-BN gate dielectric. The aim of this work is to introduce a full description of the valence bands and hole scattering mechanisms (light hole, heavy hole, spin–orbit, and subbands due to quantum confinement) in order to calculate the maximum expected hole mobility achievable in 2D gas diamond FETs.

Numerous experimental data were reported for 2D hole gas created on (001), (011), and (111) H-terminated diamond surfaces.[12–21] However, limited theoretical descriptions have been reported in the literature. Li *et al.*[22] considered the assumption of a triangular well in order to compute the different scattering rates for four scattering mechanisms such as surface impurity scattering, acoustic deformation potential scattering, nonpolar optical phonon scattering, and surface/interface roughness scattering. In their work, Li *et al.*[22] describe the valence bands assuming a triangular shape potential for the confined holes and a single density of states mass $m_d = (m_{hh}^{*3/2} + m_{lh}^{*3/2} + m_{so}^{*3/2})^{2/3}$, with m_{hh}^*, m_{lh}^*, and m_{so}^* being the hole effective masses of heavy hole, light hole, and split-off hole bands, respectively. These rough assumptions do not take into account the complex situation of holes confined in a 2D gas and cannot be used to evaluate reliably the highest mobility value expected in a 2D gas, where phonon scattering by interband and intraband mechanisms is dominant.

For the transport calculation in a 2D system, it is important to consider each band separately (m_d will be replaced here by m_{hh}^*, m_{lh}^*, and m_{so}^*), to determine their subband energy level due to the confinement in order to calculate their contribution to the different scattering mechanisms and finally to compute the mobility.

In order to calculate the mobility and carrier distribution within a 2D hole gas for (001) and (111) diamond surfaces, we solved the Schrödinger and Poisson equation self-consistently thanks to nextnano-software (supplementary material). A metal/diamond/Al_2O_3 interface has been chosen in order to accumulate a 2D hole gas at the

diamond/insulator interface. In that way, the calculations reproduce typical valence band bending and hole confinement at the diamond surface, which can be achieved by other methods (electron transfer to an insulating film or surface adsorbates). The thicknesses of the metal/diamond/Al_2O_3 stack were 70/50/1000 nm. The 2D gas is confined in the few first nanometers of diamond at the diamond/Al_2O_3 interface [as shown in Fig. 1(b) for a gate bias of −80 V]. The sheet carrier concentration has been varied thanks to the gate bias within the range of −80 V to 0 V.

The different subband energy levels, the hole wave functions, and the corresponding sheet concentrations (p_{hh}, p_{lh}, and p_{so}) have been systematically calculated within each subband for *hh*, *lh*, and *so* bands. The anisotropy of the effective masses from Ref. 23 has been included in the 2D model for (111) and (001) diamond surfaces (supplementary material). For gate bias within the range of −80 V–0 V, the total sheet hole concentration $p_S = p_{hh} + p_{lh} + p_{so}$ ranges between 5×10^{13} cm^{-3} and 5×10^{11} cm^{-3}.

Figure 1 shows the density of states, energy levels, and occupation probability $|\Psi(z)|^2$ for the first subband level for a gate bias of −80 V corresponding to a total sheet carrier concentration around 5×10^{13} cm^{-3} for (001) and (111) diamond/Al_2O_3 interfaces. The light hole and heavy hole first subbands have the deepest energy level for (001) and (111) surfaces, respectively, because of the heaviest effective masses, i.e., $m_{\perp}^{*hh}$ for (001) and $m_{\perp}^{*lh}$ for (111). The hole concentration p_{hh}, p_{lh}, and p_{so} of each band can be calculated by multiplying the density

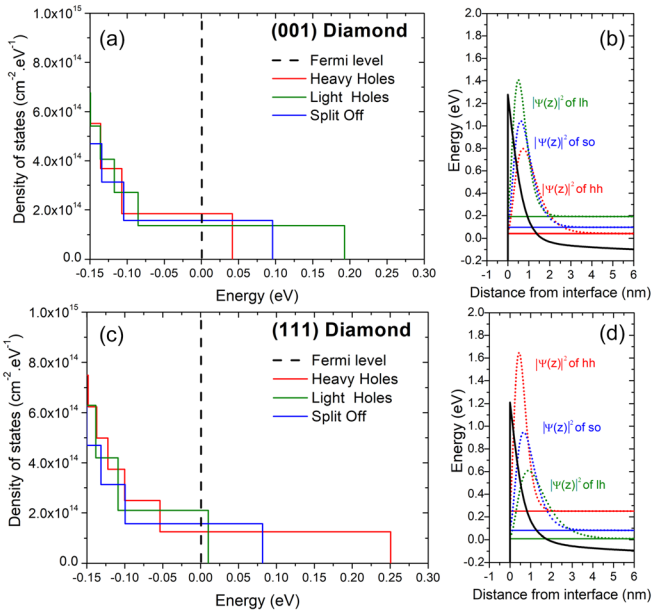

FIG. 1. (a) 2D density of states of heavy holes, light holes, and split-off valence bands of (001) diamond vs energy at a Al_2O_3/diamond interface for a gate bias of −80 V. The origin of the energy is taken at the Fermi level position. (b) Valence band edge energy of heavy holes in (100) diamond (black line) vs distance from the Al_2O_3/diamond interface for a gate bias of −80 V. The different lines represent the energy levels of the subbands (red line: heavy holes, green line: light holes, and blue line: split-off). The occupation probability $|\Psi(z)|^2$ is shown for the first level of each band (red dashed line: heavy holes, green dashed line: light holes, and blue dashed line: split-off). (c) and (d) are the same for (111) diamond.

of states by the Fermi Dirac function, where the Fermi level is taken at the origin of the energy.

The 2D hole mobility has been calculated thanks to the Boltzmann equation within the relaxation time approximation assuming parabolic bands (with effective masses given in supplementary material) and taking into account different scattering mechanisms: acoustical phonon scattering (ac), nonpolar optical phonon scattering (npo), surface impurity scattering (si), and surface roughness scattering (sr).

For the scattering mechanisms relative to phonons in the 2D case, one needs to consider interband and also intraband transitions.[26] In that case, the wave functions of holes scattered from one initial state to a final one are not always the same. These wave functions and also the corresponding overlap integrals are determined thanks to the numerical simulations described in the supplementary material. For the different scattering mechanism, we assumed the diamond static relative dielectric constant $\epsilon_s = 5.7$. For the ac scattering, the crystal mass density $\rho = 3515$ kg m^{-3}, the velocity of longitudinal acoustic phonons $v_{\parallel} = 17\,536$ m s^{-1}, and the acoustic deformation potential extracted for bulk diamond ($D_A = 8$ eV[3]) have been introduced in our calculation. For the final density of state mass m_f^*, we used the one of the subband where the hole is scattered. For the npo phonon scattering, the optical phonon energy at small values of the phonon wave vector must be considered. We used a representative phonon energy $\hbar\omega_0 = 165$ meV. This phonon energy corresponds to an average energy of the optical phonon modes at the Γ point of the Brillouin zone.[25] The effective coupling constant ($D_{npo} = 7 \times 10^9$ eV/cm), which takes into account the intraband scattering and the interband scattering in bulk diamond,[3] has been introduced in the model. Then, a summation over all the possible final states has been computed. Finally, for the surface impurity scattering, we used the procedure described in Refs. 22 and 24. We introduced the sheet hole concentration from the simulation, which is an important parameter for the screening effect. The surface impurity density $n_{imp}^{(2D)}$ and the distance d from the 2D gas to these coulombic centers are the other parameters to define. $n_{imp}^{(2D)}$ is the only parameter depending on the specific case of the diamond/insulator interface. For example, in the case of H-terminated diamond/Al_2O_3,[15] each hole is proposed to be created thanks to the transfer of an electron from the diamond valence band to any defect in the oxide close to the interface. In the case of transfer doping (for example, diamond/MoO_3[16]), the electron transfer is from the diamond valence band to the conduction band of the oxide. In both cases, $n_{imp}^{(2D)} = p_S + N_{SS}$, where N_{SS} is the surface states density (fixed charges due to trap defects at the interface).

First, we assumed that $N_{SS} \ll p_S$, i.e., $n_{imp}^{(2D)} \simeq p_S$ and $d = 0$, and we neglected the surface roughness scattering to the total mobility. The comparison between the calculated mobility for (001) and (111) diamond surfaces and experimental data from FET mobility values from the literature vs the sheet carrier concentration p_S is reported in Fig. 2. The mobility is limited by si scattering within the whole range of sheet concentrations ranging between 5×10^{11} cm^{-3} and 5×10^{13} cm^{-3}. The ac and npo scattering is almost negligible. The vicinity of the negative charges to the hole gas induces a strong decrease in the hole mobility vs the sheet carrier density. These negative charges are induced by transfer doping or by transfer to a lower energy state in the oxide. Here, by assuming $d = 0$, the contribution of the si scattering limitation is most probably overestimated to the total

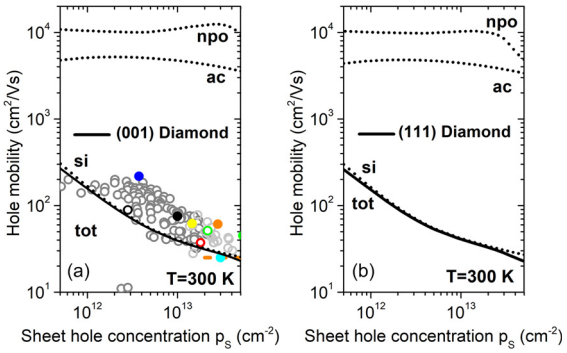

FIG. 2. Room temperature hole mobility vs sheet carrier density in (a) (001) and (b) (111) diamond field effect transistors assuming $n_{imp}^{(2D)} \simeq p_S$. Lines represent the different scattering mechanisms: acoustic phonon (ac), nonpolar optical phonon (npo), surface impurities (si) using the assumption $n_{imp}^{(2D)} = p_S$, and total mobility including all the scattering mechanisms (tot). Symbols represent the experimental data reported from the literature: dark and light gray open circles—(001) and (110) Diamond:H/Air from the study by Hirama *et al.*,[13] black full circle— (001) Diamond:H/Al_2O_3 from the study by Daicho *et al.*,[15] black open circle—(100) Diamond:H/Al_2O_3 from the study by Verona *et al.*,[19] green open circle—(001) Diamond:H/MoO_3 from the study by Russell *et al.*,[16] green full circle—(001) Diamond:H/MoO_3 from the study by Verona *et al.*,[19] yellow full circle—(001) Diamond:H/Nb_2O_5 from the study by Verona *et al.*,[19] light blue full circle—Diamond:H/ReO_3 from the study by Tordjman *et al.*,[21] red open circle—(001) Diamond:H/V_2O_5 from the study by Crawford *et al.*,[20] orange full circle—(001) Diamond:H/WO_3 from the study by Verona *et al.*,[19] orange dashed line—Diamond:H/WO_3 from the study by Tordjman *et al.*,[17] and dark blue full circle—(001) Diamond:H/ZrO_2 from the study by Liu *et al.*[18]

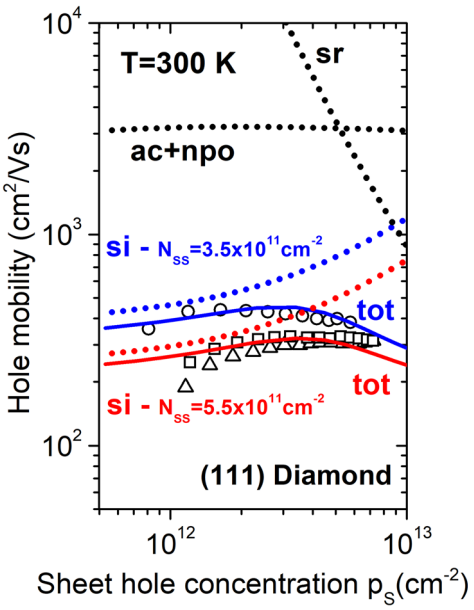

FIG. 3. Room temperature hole mobility vs sheet carrier density diamond FETs. Symbols represent the experimental data reported by Sasama *et al.*[12] for three high-mobility diamond FETs with a monocrystalline h-BN gate dielectric. Lines represent the different scattering mechanisms: acoustic phonon and nonpolar optical phonon (ac+npo), surface impurities (si) with $N_{SS} = 3.5 \times 10^{11}$ cm^{-2} (in blue) and $N_{SS} = 5.5 \times 10^{11}$ cm^{-2} (in red), surface roughness (sr) scattering with $L = 2$ nm and $\Delta = 0.25$ nm at the diamond/insulator interface, and total mobility including all the scattering mechanisms (tot).

mobility (tot). Indeed, if the negative charge distribution in the oxide is remote few Å from the interface, the 2D hole carrier mobility will be enhanced to higher values as described in Ref. 22. This is probably at the origin of the discrepancy between theoretical values and experimental ones. Our model reproduces the sheet carrier concentration dependence of the mobility, demonstrating that if the negative charges are confined too close to the interface. Any increase in the carrier concentration will be counterbalanced by a decrease in the mobility. This is the origin of the limitation of the mobility generally observed at values lower than 300 cm^2/V s in diamond FET. The hole mobility in the 2D gas is found to be almost identical for (001) and (111) diamond surfaces due to close values of in-plane effective masses, i.e., $m_{\parallel}^{*hh}$ for (001) and $m_{\parallel}^{*lh}$ for (111), of the most populated subbands.

Recently, Sasama *et al.*[12] reported a high-mobility diamond (111) FET with a monocrystalline h-BN gate dielectric. Thanks to this system, they were able to modulate the 2D hole gas sheet density thanks to a gate bias, without a significant decrease in the carrier mobility vs sheet density (see Fig. 3). Their results clearly evidenced that the negative charges, needed to ensure the neutrality of the whole system, are not accumulated in the vicinity of the hole gas but at the interface between metal and h-BN. The induced negative charges are 7 nm remote from the 2D hole gas, and so higher mobility is reached with values up to 500 cm^2/V s.

In order to theoretically describe these data, we introduced the h-BN structure in our mobility model with two si scattering mechanisms by negative charges: for the first one, $n_{imp}^{(2D)} = p_S$, negative impurities are 7 nm remote from the interface and for the second one, $n_{imp}^{(2D)} = N_{SS}$ surface state density at the interface (with N_{SS} being the adjustable parameter of the si scattering). The combination of the two si scattering mechanisms, phonon scattering mechanisms and the resulting total mobility, is shown in Fig. 3. The surface roughness scattering sr has also been added.

The numerous negative charges remote from the 2D gas are not detrimental anymore, like in GaAs/AlGaAs modulation doping transistors or GaN/AlGaN high electron mobility transistors. The charges located at 7 nm from gas have a negligible effect on the mobility. However, some traps with density in the range of $N_{SS} = 3.5 \times 10^{11}$cm^{-2}–$5.5 \times 10^{11}$cm^{-2} are present at the interface, limiting the mobility. The total mobility ranges between 250 cm^2/V s and 500 cm^2/V s. For $p_S > 3\times 10^{12}$cm^{-2}, the hole mobility decreases vs p_S probably because of the surface roughness scattering, which generally occurs when hole wave functions are confined in the vicinity of the dielectric interface. The surface roughness scattering has been introduced in the calculation with a correlation length of $L = 2$ nm.[22] The root mean square roughness height $\Delta = 0.25$ nm has been adjusted in order to fit the data as shown in Fig. 3.

This shows that the mobility can be improved up to 3000 cm^2/V s (ac + npo) for pure intrinsic phonon scattering if the interface charge density can be reduced down to a density below 10^{10} cm^{-2} and an atomically flat diamond surface ($\Delta = 0$ nm) whatever the surface orientation. These high hole mobility values are close to that of low boron doped bulk diamond.[3,27] For such high values, the hole mobility is limited by the phonon scattering mechanisms

(ac + npo) evaluated here thanks to (i) the well-established phonon constant determined previously[3] and (ii) the full description of the subband structure given above. The maximum expected 2D mobility value is higher than that of the bulk mobility because of the anisotropy of the effective masses. Indeed, the most populated subband, i.e., light holes for (001) and heavy holes for (111), has lighter in-plane effective masses $m^*_{\|}$ compared to bulk diamond density of state mass.

In conclusion, this work demonstrates that a high hole mobility up to 3000 $cm^2/V\,s$ can be achieved in 2D hole gas diamond FETs with the use of a high quality dielectric able to repel the negative charges from the 2D gas. Thanks to such high mobility, diamond FETs will be able to compete with other wide bandgap materials as SiC or GaN. In order to reach this value, a atomically flat interface needs to be achieved with trap density lower than $10^{10}\,cm^{-2}$.

See the supplementary material for the details of the model used for the calculation including the Schrödinger–Poisson equation, the effective masses, the scattering mechanisms, and the mobility.

Part of the research leading to these results was performed within the GreenDiamond project (http://greendiamond-project.eu/) and received funding from the European Community Horizon 2020 Programme (No. H2020/2014-2020) under Grant Agreement No. H2020-LCE-2014-1.640947. The authors thank Cédric Masante (Institut Néel, CNRS, Grenoble) and Gwénolé Jacopin (Institut Néel, CNRS, Grenoble) for fruitful discussions.

REFERENCES

[1]A. Hiraiwa and H. Kawarada, J. Appl. Phys. **117**, 124503 (2015).
[2]R. Berman, P. R. W. Hudson, and M. Martinez, J. Phys. C. **8**(21), L430–L434 (1975); E. A. Burgemeister, Physica B **93**, 165–179 (1978).
[3]J. Pernot, P. N. Volpe, F. Omnès, P. Muret, V. Mortet, K. Haenen, and T. Teraji, Phys. Rev. B **81**, 205203 (2010).
[4]J. Pernot, C. Tavares, E. Gheeraert, E. Bustarret, M. Katagiri, and S. Koizumi, Appl. Phys. Lett. **89**, 122111 (2006); J. Pernot and S. Koizumi, *ibid.* **93**, 052105 (2008); H. Kato, M. Ogura, T. Makino, D. Takeuchi, and S. Yamasaki, *ibid.* **109**, 142102 (2016).
[5]N. Donato, N. Rouger, J. Pernot, G. Longobardi, and F. Udrea, J. Phys. D: Appl. Phys. **53**, 093001 (2020).
[6]H. Karawada, "High voltage p-channel MOSFETs using two-dimensional hole gas," in *Power Electronics Device Applications of Diamond Semiconductors*, 1st ed., edited by S. Koizumi, H. Umezawa, J. Pernot, and M. Suzuki (Woodhead Publishing, 2018), p. 347.
[7]T. Matsumoto, H. Kato, K. Oyama, T. Makino, M. Ogura, D. Takeuchi, T. Inokuma, N. Tokuda, and S. Yamasaki, Sci. Rep. **6**, 31585 (2016).
[8]H. Umezawa, T. Matsumoto, and S.-I. Shikata, IEEE Electron Device Lett. **35**, 1112 (2014).
[9]T. T. Pham, N. Rouger, C. Masante, G. Chicot, F. Udrea, D. Eon, E. Gheeraert, and J. Pernot, Appl. Phys. Lett. **111**, 173503 (2017); T. T. Pham, J. Pernot, G. Perez, D. Eon, E. Gheeraert, and N. Rouger, IEEE Electron Device Lett. **38**, 1571 (2017).
[10]T. Iwasaki, J. Yaita, H. Kato, T. Makino, M. Ogura, D. Takeuchi, H. Okushi, S. Yamasaki, and M. Hatano, IEEE Electron Device Lett. **35**, 241 (2014).
[11]J. Pernot, "Carrier mobility in diamond: From material to devices," in *Power Electronics Device Applications of Diamond Semiconductors*, 1st ed., edited by S. Koizumi, H. Umezawa, J. Pernot, and M. Suzuki (Woodhead Publishing, 2018), p. 174.
[12]Y. Sasama, K. Komatsu, S. Moriyama, M. Imura, T. Teraji, K. Watanabe, T. Taniguchi, T. Uchihashi, and Y. Takahide, APL Mater. **6**, 111105 (2018).
[13]K. Hirama, H. Takayanagi, S. Yamauchi, J. H. Yang, H. Kawarada, and H. Umezawa, Appl. Phys. Lett. **92**, 112107 (2008).
[14]K. Hirama, H. Sato, Y. Harada, H. Yamamoto, and M. Kasu, IEEE Electron Device Lett. **33**(8), 1111 (2012); H. Sato and M. Kasu, Diamond Relat. Mater. **31**, 47 (2013).
[15]A. Daicho, T. Saito, S. Kurihara, A. Hiraiwa, and H. Kawarada, J. Appl. Phys. **115**, 223711 (2014).
[16]S. A. O. Russell, L. Cao, D. Qi, A. Tallaire, K. G. Crawford, A. T. S. Wee, and D. A. J. Moran, Appl. Phys. Lett. **103**, 202112 (2013).
[17]M. Tordjman, C. Saguy, A. Bolker, and R. Kalish, Adv. Mater. Interfaces **1**, 1300155 (2014).
[18]J. Liu, M. Liao, M. Imura, A. Tanaka, H. Iwai, and Y. Koide, Sci. Rep. **4**, 6395 (2014).
[19]C. Verona, W. Ciccognani, S. Colangeli, E. Limiti, M. Marinelli, and G. Verona-Rinati, J. Appl. Phys. **120**, 025104 (2016).
[20]K. G. Crawford, L. Cao, D. Qi, A. Tallaire, E. Limiti, C. Verona, A. T. S. Wee, and D. A. J. Moran, Appl. Phys. Lett. **108**, 042103 (2016).
[21]M. Tordjman, K. Weinfeld, and R. Kalish, Appl. Phys. Lett. **111**, 111601 (2017).
[22]Y. Li, J.-F. Zhang, G.-P. Liu, Z.-Y. Ren, J.-C. Zhang, and Y. Hao, Phys. Status Solidi RRL **12**, 1700401 (2018).
[23]N. Naka, K. Fukai, Y. Handa, and I. Akimoto, Phys. Rev. B **88**, 035205 (2013).
[24]J. H. Davies, *The Physics of Low-Dimensional Semiconductors: An Introduction* (Cambridge University Press, Cambridge, 1998), p. 365.
[25]S. A. Solin and A. K. Ramdas, Phys. Rev. B **1**, 1687 (1970).
[26]M. Lundstrom, *Fundamentals of Carrier Transport* (Cambridge University Press, 2009).
[27]P.-N. Volpe, J. Pernot, P. Muret, and F. Omnès, Appl. Phys. Lett. **94**, 092102 (2009).